astronomy

CITESCORE
2.3

Article

A Study of Four Distinct Photonic Crystal Fibers for the Maximization of the Optical Hawking Effect in Analog Models of the Event Horizon

Alfonso González Jiménez, Enderson Falcón Gómez, Isabel Carnoto Amat and Luis Enrique García Muñoz

MDPI

https://doi.org/10.3390/astronomy4040022

astronomy

MDPI

Article

A Study of Four Distinct Photonic Crystal Fibers for the Maximization of the Optical Hawking Effect in Analog Models of the Event Horizon

Alfonso González Jiménez *, Enderson Falcón Gómez, Isabel Carnoto Amat and Luis Enrique García Muñoz

Department Signal Theory and Communications, Carlos III University of Madrid, 28911 Madrid, Spain
* Correspondence: alfogonz@ing.uc3m.es

Abstract

This work aims to maximize the Hawking emission temperature arising in the optical analog model of the event horizon of an astrophysical black hole. A weak probe wave interacts with an intense ultrashort optical pulse via the Kerr effect in a photonic crystal fiber. This interaction causes the probe wave to experience an effective spacetime geometry characterized by the presence of an optical event horizon, where the analogous Hawking radiation effect arises. Here we refer to the simulated or classical version of the analog of Hawking radiation. This study considers four distinct types of photonic crystal fibers with anomalous dispersion curves that allow for maximizing the effect. Our first three numerical simulations indicate that a Hawking emission temperature of up to 361 K can be achieved with a photonic crystal fiber with two zero-dispersion wavelengths, while the emission temperature values in the original investigation are lower than 244 K. And in the fourth, we can see that we have a configuration in which the temperature can be improved up to 1027 K. Moreover, these results also emphasize the feasibility of using analog models to test the quantum effects of gravity, such as Hawking radiation produced by typical black holes, whose magnitude is far below the temperature of the cosmic microwave background (2.7 K).

Keywords: Hawking radiation; optical event horizon; photonic crystal fibers

Academic Editor: Ignatios Antoniadis

Received: 25 September 2025
Revised: 27 October 2025
Accepted: 5 November 2025
Published: 10 November 2025

Citation: González Jiménez, A.; Falcón Gómez, E.; Carnoto Amat, I.; García Muñoz, L.E. A Study of Four Distinct Photonic Crystal Fibers for the Maximization of the Optical Hawking Effect in Analog Models of the Event Horizon. *Astronomy* **2025**, *4*, 22. https://doi.org/10.3390/astronomy4040022

1. Introduction

Quantum effects of gravity may play a crucial role in describing the evolution of black holes (BHs) and the physics of the event horizon [1]. In 1974, Stephen Hawking [1,2] addressed the problem of thermal radiation produced by BHs, now widely referred to as Hawking radiation. Black holes are formed when a massive star collapses to a size below its Schwarzschild radius, i.e., $r_s = \frac{2GM}{c^2}$, where G, c, and M denote the gravitational constant, the speed of light, and the mass of the star, respectively [3]. For several years, it was generally accepted that any physical process occurring within the event horizon, i.e., the surface $r = r_s$, turned out to be undetectable to observers outside it. However, Hawking considered that the creation of real particles from virtual ones, such as photons [1], due to vacuum fluctuations occurring in the surroundings of the event horizon, could lead to an effective radiative process by BHs. In this scenario, particles, with positive energy, may either fall inward the BH or escape to infinity. In contrast, antiparticles, with negative energy, tunnel through the event horizon, where they can exist as real particles [1] and may

only move towards the BH center. This process therefore leads to the effective emission of photons, like if the BH was a hot body with temperature $T_{\mathrm{H}} = \frac{\hbar\kappa}{2\pi k_{\mathrm{B}}}$ [1], where κ represents the surface gravity [1], k_{B} denotes the Boltzmann constant, and with h being the Planck constant. Additionally, this phenomenon causes the BH to gradually lose mass due to particle emission, while its surface gravity (and, consequently, its emission temperature) increases progressively until the BH evaporates. Nevertheless, the experimental detection of Hawking radiation produced by the lightest BH possible ($M_{BH} \approx 1.39 M_{\odot}$, where $M_{\odot}$ is the solar mass [4]) remains unfeasible for two reasons: first, the Hawking temperature of the lightest BH possible is around $T_H = 85.75$ K, which lies far below the temperature of the cosmic microwave background (2.7 K); second, the evaporation timescale of such BHs is comparable to the age of the universe [1].

An alternative approach to the experimental detection of Hawking radiation could be to emulate electrodynamic and quantum properties using analogous event horizon models. There are numerous analogous models that emulate BH properties, for example [5,6]. Specifically, the dynamics of moving media have been demonstrated to reproduce spacetime geometries having effective event horizons. In 1981 [7], Unruh was the first to establish an event horizon analogy that could be replicated in a laboratory. Specifically, he did so through a fluid flow analog, demonstrating that it would be possible to emit analogous Hawking radiation in the form of sound waves. However, although this possibility exists theoretically, it has not been measured in practice. Since then, other systems have been proposed that replicate Hawking radiation, such as Bose–Einstein condensates [8–10] or nonlinear optics [11–13].

Other more recent publications propose novel techniques for detecting this type of radiation. It has been proposed to accelerate photons through tapered metamaterial optical fibers, obtaining theoretical accelerations of 10^{24} g, which is equivalent to a theoretical effective temperature of $T_U \sim 4000$ K (Unruh temperature), but in practice, this type of experiment presents several problems [14]. An alternative way to detect radiation in this sense is to observe the loss of entanglement of photons due to T_U. This technique has been attempted experimentally in [15], but only accelerations below 30 g have been obtained, which would be equivalent to a temperature of $T_U \sim 10^{-18}$ K. As we can see, there is a huge gap between the theoretically predicted maxima and the experimental values.

Attempts have also been made to detect the Unruh effect by accelerating electrons. In this case, accelerations to energies on the order of GeV have currently been achieved at distances of a few mm [16]. In this case, the Unruh radiation power must be compared with the Larmor radiation power. In these experiments, the ratio of the Unruh and Larmor powers obtained is $P_U/P_L \sim 10^{-10}$ [17]. The radiation density of thermal energy can be improved by using hyperbolic metamaterials, where the Planck expression for radiation increases by several orders of magnitude. However, through the use of these materials, the value would only be improved by $P_U/P_L \sim 10^{-5}$ in the most optimistic case [17]. However, the use of metamaterials in this case has the disadvantage that direct interaction between the accelerated electron and the metamaterial itself must be avoided, which is very complex experimentally.

All of these different methods provide a way to measure T_U, but it would actually be the Unruh temperature, not the Hawking temperature. Although they can be related through Einstein's equivalence principle, in this case, no event horizon is simulated, unlike the original optical method [11].

Of these methods, the optical one is expected to have the highest particle emission, the highest effective temperature, the highest experimental sensitivity, and the absence of a thermal background that would affect its measurement [12]. Attempts have been made to establish theoretical designs for optical experiments to obtain results through numerical

simulations. But unfortunately, the dispersion relation of usable photonic crystal fibers (PCFs) cannot be easily expressed in a Sellmeier formula [12]. This is due to the lack of theoretical knowledge of the fibers. Dispersion curves are obtained from experimental measurements; these must be verified experimentally in the laboratory. The result is a discrete set of data points that describe the fiber dispersion, rather than an analytical relationship like the ones current algorithms can handle [12].

This work focuses on the class of optical analog models, where a pulse traveling through a photonic crystal fiber (PCF) induces a propagating perturbation of the fiber's refractive index profile via the Kerr effect. As a result, probe signals propagating in the PCF experience an effective spacetime geometry with an artificial event horizon. In this case a continuous-wave probe is used, since alternative techniques employ a pulsed probe [13]. For this reason, we are seeking experimental alternatives that are believed to improve upon previously obtained results. Starting from the original experimental setup, a preliminary theoretical study will be conducted, varying the optical fibers used to seek an improvement over the results previously obtained in this specific experimental setup, with a view to future replication of the experiment.

The simplest way (with respect to setup) to improve the results obtained previously is by replacing the optical fiber used. Furthermore, it would be the most economical way to obtain different results because the other method is extremely expensive. The other way to obtain different results would be to change the laser that creates the main pulse in the fiber. The laser considered in this article (and used in almost all experiments of this type [11,12]) is a Ti–Sapphire laser with a wavelength $\lambda = 803\,\text{nm}$. This choice is not accidental, and changing this laser would require redesigning the entire experimental setup, in addition to the extremely high cost of each laser of this type. Very powerful lasers are needed, as the second-order effects (Kerr effect) of the fibers are present. Therefore, modifying the properties of optical fibers has been considered the simplest and most viable way to improve the values obtained previously, as well as to obtain a wide range of results, which can provide very valuable additional information about the Hawking radiation phenomenon.

Considering the practical limitations of the experimental instrumentation, four distinct PCFs, including existing commercial options and well-characterized theoretical designs, are considered in our study. As a novelty with respect to previous experiments, this paper uses PCFs doped with different materials [18] or with different geometries [19,20] than those previously used in experiments of this type [11–13], demonstrating that they can improve these previous results with more conventional fibers. Following the analytical methods designed/proposed by Philbin et al. [11], the analog Hawking radiation emission is calculated for experiments utilizing each PCF. In particular, four distinct PCFs are considered, and the Hawking temperature due to the interaction between the probe wave and the optical event horizon is calculated. Our findings indicate that the fibers chosen can lead to analog emission temperatures with magnitudes exceeding those levels reported in previous investigations [11,12].

This paper is organized as follows: Section 2 addresses the formation of optical event horizons in optical analog models, the experimental setup, and the methods employed in this work. Subsequently, the results of the numerical experiments are discussed in Section 3. Finally, Section 4 summarizes the conclusions and outlines the future perspectives of this work.

2. Optical Analog of the Event Horizon

This section introduces the fundamentals of the emulation of the Hawking effect using optical analog models. Section 2.1 discusses the formation of optical event horizons in

microstructured fibers. The key result of this section is an expression for the Hawking emission temperature (13). Subsequently, the experimental configuration corresponding to our numerical experiments is outlined in Section 2.2. Finally, Section 2.3 describes the methodology followed in this work.

2.1. Formation of Optical Event Horizons in Microstructured Fibers

The formation of optical event horizons arises when an intense ultrashort optical pulse interacts with a weak probe wave in a PCF [11]. Consider a PCF aligned in the z-axis of the laboratory rest frame. A pulse with the central frequency ω_p propagates in the positive z-axis at the group velocity $u = c/n$. This pulse will have an intensity high enough for nonlinear effects to be relevant. As the pulse propagates along the fiber, its refractive index, n_0, gains an additional contribution $\delta n(z,t) \propto I(z,t)$ due to the Kerr effect, where $I(z,t)$ represents the instantaneous intensity profile of the pulse along the PCF [11]. Therefore, the nonlinear effects of the pulse cause it to reduce its propagation velocity in the fiber since $n > n_0$. As for the probe wave, the following assumptions are made: (a) it is monochromatic, with input frequency $\omega_{\text{cw-in}}$; (b) its group velocity, $V_g = c/n_0$, is slightly higher than the group velocity of the pulse; (c) its nonlinear effects and backreaction onto the pulse are negligible [11], i.e., $I(z,t) \to 0$ and, therefore, $\delta n(z,t) \to 0$; and (d) it co-propagates with the pulse. Consequently, as both the pulse and the probe wave propagate in the PCF, the effective refractive index experienced by the probe wave in the PCF will assume the form:

$$n(z,t) = n_0 + \delta n(z,t) \tag{1}$$

As the probe wave approaches the trailing edge of the pulse, it will increasingly feel the perturbation of the refractive index δn, and will therefore slow down until it reaches the same speed as the pulse but without exceeding it. This phenomenon is exactly the same as that which occurs at the horizon of a white hole [11,21]. Thus, an optical white hole horizon arises in the trailing edge of the perturbation δn. For our purpose, which is to obtain intense analog Hawking radiation emissions, we will focus on a white hole instead of a black hole. We choose white holes due to the self-steepening effect, which results from including dispersion in the nonlinear term of the pulse propagation equation [22]. In this case, the pulse curvature (and, therefore, the variation in δn) will be steeper in those cases.

Let A_{probe} be the potential vector of the probe wave in the PCF, which can be expressed as follows:

$$A_{\text{probe}}(\omega, x, y, z) = A(\omega, z)U(\omega, x, y) \tag{2}$$

Here, $U(\omega, x, y)$ describes the distribution of the potential vector on the cross-section of the PCF, while $A(\omega, z)$ is a function that contains the variation in the potential vector along the fiber. It can be easily demonstrated [11] that, in the co-moving reference frame, (τ, ς), of the pulse:

$$\tau = t - \frac{z}{u} \tag{3}$$

$$\varsigma = \frac{z}{u} \tag{4}$$

the function A will satisfy the following homogeneous wave equation:

$$\partial \cdot g^{\mu\nu} \partial \circ A = 0 \tag{5}$$

where the Einstein summation convention is assumed over repeated indices, and the term $g^{\mu\nu}$ (where μ and ν are the parameters of the metric components), given by

$$g^{\mu\nu} = \begin{pmatrix} 1 & -1 \\ -1 & 1 - u^2 n^2 / c^2 \end{pmatrix} \tag{6}$$

represents the effective metric tensor induced by the spacetime-varying refractive index of the PCF. Notice that this effective spacetime geometry resembles that of moving media [7,11,21]. Hence, we use the theory of electromagnetic wave propagation in moving media (see [21], p. 217) to carry out the electrodynamic analysis of the formation of optical event horizons in PCFs. To this end, we assume that the electromagnetic properties of the PCF satisfy the impedance-matching conditions [21]:

$$\frac{\epsilon}{\epsilon_0} = \frac{\mu}{\mu_0} = n(z,t) \tag{7}$$

According to (6), the formation of optical event horizons occurs when the phase velocity of the probe wave matches the group velocity of the pulse [11]:

$$\frac{c}{n} = u \tag{8}$$

In this scenario, the velocity of the probe wave with respect to the laboratory frame can be estimated from the Einstein addition theorem of velocities in moving media [21]

$$v_{\pm} = \frac{u \pm \frac{c}{n}}{1 \pm \frac{u}{cn}} \tag{9}$$

We define our co-moving coordinate system such that the horizon is located at $\tau = 0$. Subsequently, we expand v_+ to linear order in the distance τ from the horizon, e.g., $v_{\pm} = \alpha z$, where α is the so called analog surface gravity (see [21], p. 222). The α parameter determines the magnitude of the Hawking radiation, and it is given by the following expression [21]:

$$\alpha = -\frac{1}{\delta n}\frac{d\delta n}{d\tau} \tag{10}$$

The reader is referred to Refs. [11,21] for further details on the derivation of the α parameter. Then, the Hawking temperature, as measured in the laboratory frame [21], is expressed as

$$k_B T_H = \frac{\hbar \alpha}{2\pi} \tag{11}$$

Notice that, according to (11) and (10), the magnitude of the Hawking radiation and, therefore, the particle production rate depend solely on the acuity of the pulse. This is an exponentially accurate approximation of geometric optics until the condition

$$\left|\frac{\partial T_c}{\partial \tau}\right| << 1 \qquad \text{for} \qquad T_c = \frac{2\pi}{\omega} \tag{12}$$

is violated in the horizon [23]. Here, the cycle T_c plays the role of wavelength. For waves with the logarithmic asymptotics expressed by the equation $\varphi = -\int(\omega d\tau + \omega' d\zeta)$, we have $\omega = \omega'/(\alpha'\tau) = \omega_{\text{cw-out-2}}/(\alpha\tau)$, where $\omega_{\text{cw-out-2}}$ is the laboratory frequency of the outgoing wave far from the horizon. Since $T_c = \frac{2\pi}{\omega}$, we see that $\frac{\partial T_c}{\partial \tau}$ reaches unity at a Hawking temperature when ([11] Supporting Online Material p. 16)

$$k_B T_H = \frac{\hbar \omega_{\text{cw-out-2}}}{(2\pi)^2} \tag{13}$$

The Hawking temperature depends on the time-dependent change in the refractive index variation induced by the pulse in the fiber (δn), as indicated in Equations (10) and (11).

This is simply the verticality of the pulse. For a completely vertical pulse (logarithmically asymptotic), the maximum value (13) will be obtained. However, it is clear that these values are directly proportional. Therefore, increasing the value of (13) should increase the value actually measured in the experiment, and will certainly improve the results of previous experiments. The extent to which this depends on the fiber is that this phenomenon depends on the refractive index n, whose dependence is implicit in the dispersion diagrams used.

Furthermore, the frequency in the co-moving frame, ω', relates to the central frequency of the probe wave, as measured in the laboratory frame via the Doppler formula [11,21]

$$\omega' = \left(1 - \frac{nu}{c}\right)\omega \tag{14}$$

The light on either side of the horizon consists of an ensemble of photon-number eigenstates with probability $Z^{-1}e^{-2n\pi\omega'/\alpha'}$, with an Einstein–Podolski–Rosen (E.P.R.) quantum state $|vac\rangle = Z^{-1/2}\sum_{n=0}^{\infty} e^{-n\pi\omega'/\alpha'}|n,n\rangle$, where $Z = (1 - e^{-2\pi\omega'/\alpha'})^{-1}$ ([11] Supporting Online Material p. 16).

Furthermore, since we are dealing with quantum processes, the appearance of tunneling in the pulse is possible. To the probe wave, the soliton is a constant one-dimensional potential, for which the transmission and reflection coefficients can be found. But for small detunings there is negligible tunneling and the probe is nearly perfectly reflected. For more details (see [12] Section 5.3.2).

2.2. Experimental Setup Description

The scheme of the experimental setup for testing the formation of optical event horizons in PCFs, initially proposed by Leonhardt et al. [11,21], is illustrated in Figure 1. The probe wave, with an infrared (IR) central wavelength λ_{cw}, is emitted from a continuous-wave tunable laser. Then it is reflected off a diffraction grating (G) to suppress fluorescence. The beam is steered into a microstructured fiber (MF) by a polarizing beam splitter (PBS), a half-wave plate (HWP), and a coupling lens (L). The intense ultrashort optical pulses, with a central wavelength $\lambda_0 = 803\,\text{nm}$, are generated by a Ti–Sapphire laser. At the output of the PCF, the intense ultrashort pulses are removed by a dichroic filter (DF), and the spectrum of the probe wave is taken through a standard single-mode fiber (SMF).

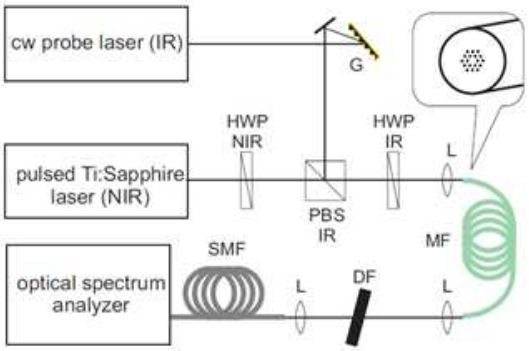

Figure 1. Experimental setup to test the formation of optical event horizons using a PCF. This figure has been taken from the Supplemental Material of Ref. [11].

2.3. Methods

After the foregoing, we analyze the conditions necessary for the formation of the optical event horizon in a PCF, determining these conditions from the dispersion properties of the PCF; see Section 2.1. In the same context, we discuss additional effects on light propagation arising from dispersion. Finally, we address the calculation of the theory light spectrum at the output of the PCF (see Figure 1).

The dispersion curve of the PCF, $D(\lambda)$, with a wavelength of the pump λ_0, relates to the group velocity of light in the fiber, $v_g(\lambda_0)$, through the following integral [11]

$$\int_{\lambda_0}^{\lambda} D(\lambda)d\lambda = \frac{1}{v_g(\lambda)} - \frac{1}{v_g(\lambda_0)} \tag{15}$$

The fulfillment of condition (8) along with the experimental instrumentation available for the experiment and Equation (15) define the characteristic of the dispersion properties of the PCF that can be utilized in the experiment. In particular, condition (8) suggests that Equation (15) must vanish. This entails that a point of zero dispersion in the dispersion curve of the PCF must occur between the wavelength of the probe and the pulse. The probe wavelength at which this integral vanishes is called the velocity-matched wavelength of the group λ_m. That is, for $\lambda = \lambda_m$, Equation (15) will vanish. Additionally, optical instrumentation must be capable of detecting the wavelengths involved in the experiment. Nonlinear optical systems exhibit instability that leads to modulation of the steady state as a result of an interplay between nonlinear and dispersive effects. This requires an optical fiber with anomalous dispersion and manifests itself as the breaking up of continuous wave radiation into a train of ultrashort pulses. Photons produced at the idler frequency, since they have a different frequency to that of the probe ($\omega_{\mathrm{cw-in}}$) and a higher value, will be said to be blue-shifted, as shown at the end of Section 2.1. This new frequency will determine the maximum value of the Hawking temperature in our model (13), which we define as $\omega_{\text{cw-out-2}}$:

$$\omega_{\text{cw-out-2}} = 2\omega_{\mathrm{m}} - \omega_{\mathrm{cw-in}} \tag{16}$$

However, light propagating in the PCF also experiences Raman-induced soliton self-frequency shift [11]. As a result, the central wavelength of the pulse, the probe wave, and that of the group velocity-matched wavelength are red-shifted. The wavelength shift for the pulse is $\delta\lambda_0 = 4\,\mathrm{nm}$ [11]. Similarly, the frequencies of both the probe wave $\omega_{\mathrm{cw-in}}$ and the group velocity-matched frequency ω_{m} are calibrated accordingly by adding $\delta\omega_{\mathrm{cw}}$, where

$$\delta\omega_{\mathrm{cw}} = -\frac{\delta\lambda_{\mathrm{cw}}}{\lambda_{\mathrm{m}}\omega_{\mathrm{m}}} \tag{17}$$

where $\delta\lambda_{\mathrm{cw}}$ is calculated using

$$\delta\lambda_{\mathrm{cw}} = \frac{D(\lambda_0)}{D(\lambda_{\mathrm{m}})}\delta\lambda_0 \tag{18}$$

The effect of Raman-induced frequency shift must be considered in (16). Then, the spectrum of the probe wave at the output of the PCF [11] may be calculated using the following expression

$$\tilde{A} = \frac{\eta_{\mathrm{r}}A_0}{\pi(\omega+\omega_{\mathrm{s}}-2\omega_{\mathrm{m}})}\left[e^{iq(\omega-\omega_{\mathrm{m}})^2} - e^{iq(\omega_{\mathrm{s}}-\omega_{\mathrm{m}})^2}\right] +$$

$$+\frac{A_0}{\pi(\omega-\omega_{\mathrm{s}})}G\left[\sqrt{iq}(\omega-\omega_{\mathrm{m}})\right] - \frac{A_0}{\pi(\omega-\omega_{\mathrm{s}})}G\left[\sqrt{iq}(\omega_{\mathrm{s}}-\omega_{\mathrm{m}})\right] \tag{19}$$

where $\omega_{\mathrm{s}} = \omega_{\text{cw-out-1}}$ is the red-shifted central frequency of the probe wave due to the interaction of the probe wave with the optical event horizon; η_{r} is the reduced efficiency, which is a phenomenological quantity; we use $\eta_{\mathrm{r}} = 0.8$ [11]; $G(x) = e^{-x^2}\cdot \mathrm{erfi}(x)$; $A_0 = 4.1\times 10^{12}\sqrt{Ws}$ [11] is the amplitude of the probe wave at the input; and the quantity q is determined from:

$$q = \frac{\pi c|D_{\mathrm{m}}|L}{\omega_{\mathrm{s}}^2} \tag{20}$$

Here $L = 1.5\,\mathrm{m}$ is the length that will be considered in all the PCFs studied. In this way, we have established everything necessary, analytically, to be able to optimize the result of Hawking radiation in the fiber optic analog.

3. Results

This section presents the results obtained in our study. Four different types of PCFs have been considered in this work: (i) C-PCF 10% GeO2 [18]; (ii) fiber with two zero-dispersion wavelengths [24]; (iii) fiber with large anomalous dispersion and air holes [19]; (iv) an air–silica nanowire [20]. These PCFs were selected because the zero-dispersion point of their dispersion curves occurs close to the operating wavelength of the laser pulse, so that the blue-shifted pulse, i.e., the analog Hawking radiation emission, can be detected by our optical instrumentation when the experiment is implemented, according to condition (8) and Equation (15). Furthermore, only existing commercial options and well-characterized theoretical designs have been considered, since optimizing the dispersive properties of PCFs is a problem beyond the scope of this work, and in addition, the purpose of this work only encompasses the selection of a PCF that allows us to improve the magnitude of the analog Hawking radiation that can be achieved in the experiment proposed by Philbin and Ulf [11]. Despite this, this problem, alongside the physical implementation of the aforementioned well-characterized theoretical PCF design, will be considered in future work.

3.1. First Case: GeO2 Fiber

This section considers the real fiber C-PCF 10% GeO2 [18], whose dispersion curve is shown in Figure 2a. Following the methodology outlined in Section 2.3, we obtain the dispersion parameters displayed in Table 1. In addition, notice that the shadowed area in the dispersion curve stems from the fulfillment of condition (8), as discussed in Section 2.3.

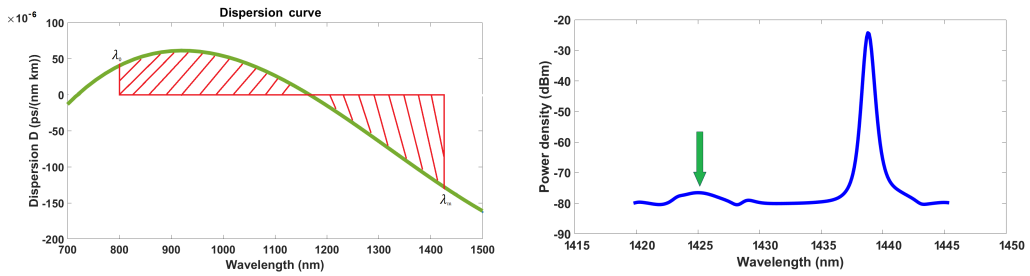

(**a**) (**b**)

Figure 2. Figures of the first case. (**a**) Dispersion curve in the theoretical fiber C-PCF 10% GeO2. Taken from [18]. (**b**) Representation of the spectrum at the output of the PCF (after pulse removal).

As for the spectrum at the output of the PCF, it will consist of two spectral components at the following wavelengths: (a) $\lambda_{\text{cw-out-1}}$, the red-shifted central wavelength of the probe wave, and (b) $\lambda_{\text{cw-out-2}}$, the blue-shifted central wavelength of the probe wave due to the interaction of the probe wave with the optical event horizon (see Section 2.3). Using $\lambda_{\text{cw-in}} = 1439\,\mathrm{nm}$ and applying Equations (18) and (17) lead to $\lambda_{\text{cw-out-1}} = 1438\,\mathrm{nm}$ and $\lambda_{\text{cw-out-2}} = 1425\,\mathrm{nm}$, while Figure 2b shows the ensuing spectrum at the output of the PCF (after removing the contribution due to the intense ultrashort optical pulses), as computed using (19). Notice the blue-shifted pulse, which is indicated by the green arrow. Finally, the Hawking temperature corresponding to the blue-shifted probe wave with the central wavelength at $\lambda_{\text{cw-out-2}}$ is computed using (13), leading to $T_{\mathrm{H}} = 256\,\mathrm{K}$.

Table 1. Dispersion parameters for GeO2 fiber.

Parameter	Value	Expressions
λ_0 (nm)	803	
D_0 $(\frac{\text{ps}}{\text{nm}\cdot\text{km}})$	41×10^{-6}	
λ_m (nm)	1433	(8) and (15)
D_m $(\frac{\text{ps}}{\text{nm}\cdot\text{km}})$	-128×10^{-6}	(8) and (15)
$\delta\lambda_{cw}$ (nm)	-1.2752	(18)
$\lambda_{cw\text{-}in}$ (nm)	1439	
$\lambda_{cw\text{-}out\text{-}1}$ (nm)	1438	
$\lambda_{cw\text{-}out\text{-}2}$ (nm)	1425	

3.2. Second Case: Fiber with Two Zero-Dispersive Wavelengths

In this case, we study the formation of optical event horizons in a real PCF with two zero-dispersive wavelengths, introduced in [24]. The dispersion curve of this PCF is shown in Figure 3a. Similar procedures like those employed in the previous section are also followed here. Our analysis of this PCF leads to the results gathered in Table 2.

The spectrum at the output of the PCF, after removal of the intense ultrashort optical pulses, is displayed in Figure 3b, where we can distinguish two pulses—one with the central wavelength at $\lambda_{cw\text{-}out\text{-}1}$ (red-shifted probe wave) and another at $\lambda_{cw\text{-}out\text{-}2}$ (blue-shifted probe wave), which originated due to the interaction of the probe wave with the optical event horizon. For this case, the Hawking emission temperature corresponding to the blue-shifted component [indicated by the green arrow in Figure 3b] at $\lambda_{cw\text{-}out\text{-}2}$ turns out to be $T_H = 361$ K.

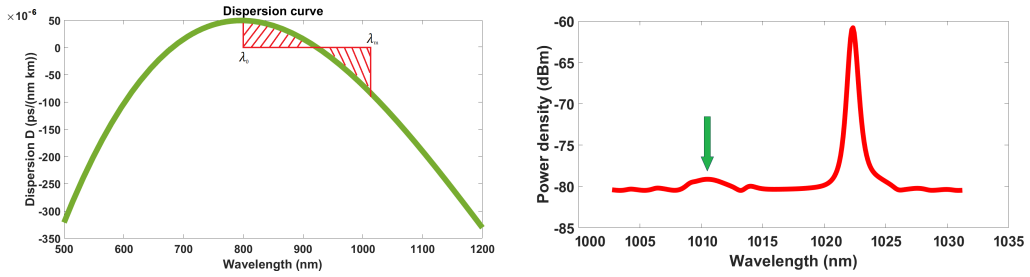

(**a**) (**b**)

Figure 3. Figures of second case. (**a**) Dispersion curve of a PCF with two zero-dispersive wavelengths. Taken from [24]. (**b**) Representation of the spectrum at the output of the PCF (after pulse removal).

Table 2. Dispersion parameters for fiber with two zero-dispersive wavelengths.

Parameter	Value	Expressions
λ_0 (nm)	803	
D_0 $(\frac{\text{ps}}{\text{nm}\cdot\text{km}})$	49×10^{-6}	
λ_m (nm)	1017	(8) and (15)
D_m $(\frac{\text{ps}}{\text{nm}\cdot\text{km}})$	-88.5×10^{-6}	(8) and (15)
$\delta\lambda_{cw}$ (nm)	-2.219	(18)
$\lambda_{cw\text{-}in}$ (nm)	1025	
$\lambda_{cw\text{-}out\text{-}1}$ (nm)	1023	
$\lambda_{cw\text{-}out\text{-}2}$ (nm)	1010	

3.3. Third Case: Fiber with Large Anomalous Dispersion and Air Holes

In this case, we consider a simulated PCF with large anomalous dispersion and air holes, described in [19]. Its dispersion curve is shown in Figure 4a, while the results of its

analysis are listed in Table 3.

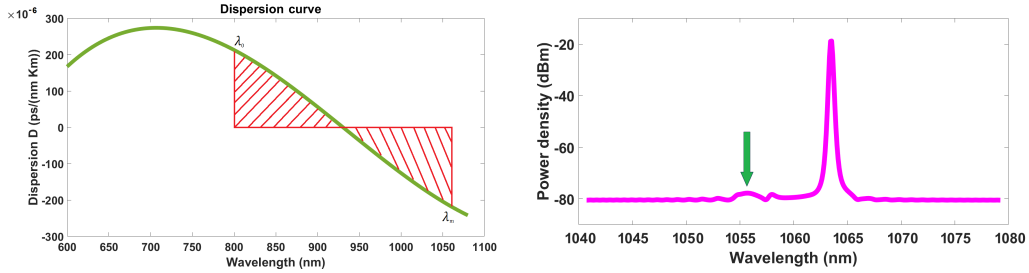

(**a**) (**b**)

Figure 4. Figures of third case. (**a**) Dispersion curve of a PCF with large anomalous dispersion and air holes. Taken from [19]. (**b**) Representation of the spectrum at the output of the PCF (after pulse removal).

Table 3. Dispersion parameters for fiber with large anomalous dispersion and air holes.

Parameter	Value	Expressions
λ_0 (nm)	803	
D_0 $(\frac{\text{ps}}{\text{nm·km}})$	212.1×10^{-6}	
λ_{m} (nm)	1060	(8) and (15)
D_{m} $(\frac{\text{ps}}{\text{nm·km}})$	-218.0×10^{-6}	(8) and (15)
$\delta\lambda_{\text{cw}}$ (nm)	-1.94	(18)
$\lambda_{\text{cw-in}}$ (nm)	1066	
$\lambda_{\text{cw-out-1}}$ (nm)	1064	
$\lambda_{\text{cw-out-2}}$ (nm)	1055	

The output spectrum is computed using (19); see Figure 4b. Here, the blue-shifted pulse is similarly indicated by a green arrow. The Hawking temperature corresponding to this pulse is $T_{\text{H}} = 346$ K. These three previous cases are likely to improve the results provided in the original article [11] in future variations of the experiments.

3.4. Fourth Case: Air–Silica Nanowire

Finally, we will use another real fiber to try to improve one of the most recent results [12] and its analogous Hawking temperature. To do this, we will use an air–silica nanowire [20]. Here, the authors prove that it is possible to establish solitons in this type of fiber. Specifically, for our calculations, we will take the dispersion curve at a wavelength of 800 nm (blue curve in Figure 1 in [20]). This is the wavelength at which the laser used in [11] works. To improve the original result (just by changing the fiber), it would be necessary to find a configuration that would minimize the zero dispersion wavelength (ZDW). This is precisely what the author does in [12] (Chapter 5) to improve the previous results of [11], working with $T_H = 685$ K. In the dispersion curve that we will take here from the air–silica nanowire [20], the ZDW is very delayed, being about 150 nm lower than the value for the fiber taken for the experiment in [12]. The dispersion curve is shown in Figure 5a, while the results of its analysis are listed in Table 4.

Recalculating the output spectrum using (19), as shown in Figure 5b, the Hawking temperature corresponding to this pulse is $T_{\text{H}} = 1027$ K. If the soliton wavelength (λ_0) were further increased, the analogous temperature obtained could be slightly higher, since, as can be seen in [20] (Figure 1), slightly increasing this value would slightly favor this result. This configuration increases the temperature but may be more difficult to detect

since the values differ little from one another. In addition, a probe laser with a wavelength around 355 nm will be needed.

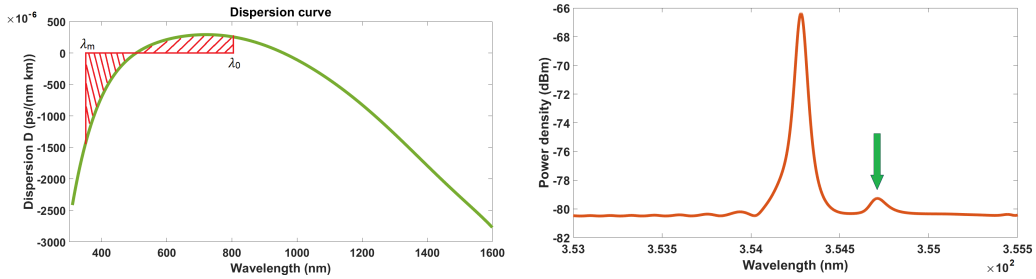

(**a**) (**b**)

Figure 5. Figures of fourth case. (**a**) Dispersion curve of a PCF air–silica nanowire. Taken from [20]. (**b**) Representation of the spectrum at the output of the PCF (after pulse removal).

Table 4. Dispersion parameters for air–silica nanowire.

Parameter	Value	Expressions
λ_0 (nm)	803	
D_0 $(\frac{\text{ps}}{\text{nm·km}})$	273×10^{-6}	
λ_{m} (nm)	355	(8) and (15)
D_{m} $(\frac{\text{ps}}{\text{nm·km}})$	-1333×10^{-6}	(8) and (15)
$\delta\lambda_{\text{cw}}$ (nm)	-0.819	(18)
$\lambda_{\text{cw-in}}$ (nm)	355.08	
$\lambda_{\text{cw-out-1}}$ (nm)	354.3	
$\lambda_{\text{cw-out-2}}$ (nm)	354.9	

4. Conclusions

In this article, a numerical study is carried out to maximize the magnitude of the Hawking effect arising in optical analog models of the event horizon using PCFs. Our study is based on the original experiment initially proposed by Leonhardt and Philbin in [11], where a Hawking emission temperature of $T_{\text{H}} = 244$ K was achieved while using a fiber NL-PM-750B. To maximize the magnitude of the optical Hawking effect, there are different approaches, such as using PCFs with anomalous dispersion curves that allow for maximizing the effect, increasing the output power from both a Ti-sapphire laser and/or a probe-wave laser. Nevertheless, only using different PCFs represents the most promising and affordable method.

Our study encompasses four distinct types of PCFs (Table 5): (i) C-PCF 10% GeO2 [18]; (ii) fiber with two zero-dispersive wavelengths [24]; (iii) fiber with large anomalous dispersion and air holes [19]; and (iv) an air–silica nanowire [20]. The findings indicate that an optical Hawking emission temperature of up to 1027 K can be achieved using the air–silica nanowire considered in case (iv), which, as detailed in Section 3.2, is considerably higher than the values used by M. J. Jacquet [12] and Leonhardt and Philbin [11].

This work addressed both the theoretical and numerical aspects of the experiment. Future perspectives include the experimental validation of our results; the design of bespoke PCFs to maximize the optical Hawking effect taking place in these analog models; a numerical simulation of the experiment using in-house full-wave solvers; and exploring other quantum effects, such as tunneling on the event horizon.

Table 5. Summary table with the T_H values of each fiber.

Fiber	Hawking Temperature (K)
C-PCF 10% GeO2	256
Fiber with two zero-dispersive wavelengths	361
Fiber with large anomalous dispersion and air holes	346
Air–silica nanowire	1027

Author Contributions: Conceptualization, A.G.J. and L.E.G.M.; methodology, A.G.J.; software, A.G.J.; validation, A.G.J.; formal analysis, A.G.J.; investigation, A.G.J. and L.E.G.M.; resources, L.E.G.M.; data curation, A.G.J.; writing—original draft preparation, A.G.J.; writing—review and editing, A.G.J., I.C.A., and E.F.G.; visualization, A.G.J. and E.F.G.; supervision, E.F.G. and L.E.G.M.; project administration, L.E.G.M.; funding acquisition, L.E.G.M. All authors have read and agreed to the published version of the manuscript.

Funding: This research was funded by Agencia Estatal de Investigacion (grant number: PID2019-109984RB-C41).

Data Availability Statement: The original contributions presented in this study are included in the article. Further inquiries can be directed to the corresponding author.

Conflicts of Interest: The authors declare no conflicts of interest.

References

1. Hawking, S.W. Black hole explosions? *Nature* **1974**, *248*, 30–31. [CrossRef]
2. Hawking, S.W. Particle creation by black holes. *Commun. Math. Phys.* **1975**, *43*, 199–220. [CrossRef]
3. Novikov, I.; Frolov, V. *Physics of Black Holes*; Springer Science & Business Media: Berlin/Heidelberg, Germany, 2013; Volume 27.
4. Chandrasekhar, S. The maximum mass of ideal white dwarfs. *Astrophys. J.* **1931**, *74*, 81. [CrossRef]
5. Falcon-Gomez, E.; De Falco, V.; Atia Abdalmalak, K.; Amor-Martin, A.; De La Rubia, V.; Santamaria-Botello, G.; García, Muñoz, L.E. Interactions between linear polarized gravitational waves and electromagnetic waves in an electromagnetic analog of gravity. *Phys. Rev. D* **2023**, *107*, 124042. [CrossRef]
6. Falcón-Gómez, E.; De Falco, V.; Atia Abdalmalak, K.; Amor-Martin, A.; De La Rubia, V.; Santamaria-Botello, G.; Munoz, L.E.G. Fully metallic geodesic lenses as analog electromagnetic models of static and spherically symmetric gravitational fields. *Phys. Rev. D* **2024**, *110*, 084002. [CrossRef]
7. Unruh, W.G. Experimental black-hole evaporation? *Phys. Rev. Lett.* **1981**, *46*, 1351. [CrossRef]
8. Garay, L.J.; Anglin, J.R.; Cirac, J.I.; Zoller, P. Sonic Analog of Gravitational Black Holes in Bose-Einstein Condensates. *Phys. Rev. Lett.* **2000**, *85*, 4643–4647. [CrossRef]
9. Giovanazzi, S.; Farrell, C.; Kiss, T.; Leonhardt, U. Conditions for one-dimensional supersonic flow of quantum gases. *Phys. Rev. A* **2004**, *70*, 063602. [CrossRef]
10. Giovanazzi, S. Hawking radiation in sonic black holes. *Phys. Rev. Lett.* **2005**, *94*, 061302. [CrossRef] [PubMed]
11. Philbin, T.G.; Kuklewicz, C.; Robertson, S.; Hill, S.; Konig, F.; Leonhardt, U. Fiber-optical analog of the event horizon. *Science* **2008**, *319*, 1367–1370. [CrossRef] [PubMed]
12. Maxime J. *Negative Frequency at the Horizon*; Springer: Berlin/Heidelberg, Germany, 2018.
13. Drori, J.; Rosenberg, Y.; Bermudez, D.; Silberberg, Y.; Leonhardt, U. Observation of stimulated hawking radiation in an optical analogue. *Phys. Rev. Lett.* **2019**, *122*, 010404. [CrossRef] [PubMed]
14. Smolyaninov, I. Giant unruh effect in hyperbolic metamaterial waveguides. *Opt. Lett.* **2019**, *44*, 2224–2227. [CrossRef] [PubMed]
15. Fink, M.; Rodriguez-Aramendia, A.; Hsteiner, J.; Ziarkash, A.; Steinlechner, F.; Scheidl, T.; Fuentes, I.; Pienaar, J.; Ralph, T.C.; Ursin, R. Experimental test of photonic entanglement in accelerated reference frames. *Opt. Lett.* **2017**, *8*, 15304. [CrossRef]
16. Howl, R.; Penrose, R.; Fuentes, I. Exploring the unification of quantum theory and general relativity with a bose–einstein condensate. *New J. Phys.* **2019**, *21*, 043047. [CrossRef]
17. Smolyaninov, I. Enhancement of unruh effect near hyperbolic metamaterials. *Europhys. Lett.* **2021**, *133*, 18001. [CrossRef]

18. Nguyen, T.T. Optimization of dispersions in geo2-doped photonic crystal fibers with square lattice. *VNU J. Sci. Math.-Phys.* **2023**, *39*. [CrossRef]
19. Liu, J. Large anomalous dispersion at short wavelength and modal properties of a photonic crystal fiber with large air holes. *IEEE J. Quantum Electron.* **2006**, *42*, 961–968. [CrossRef]
20. Salem, A.; Cherif, R.; Zghal, M. Low-energy single-optical-cycle soliton self-compression in air-silica nanowires. *J. Nanophotonics* **2011**, *5*, 59506. [CrossRef]
21. Leonhardt, U. *Essential Quantum Optics: From Quantum Measurements to Black Holes*; Cambridge University Press: Cambridge, UK, 2010.
22. Agrawal, G. *Nonlinear Fiber Optics*; Academic Press: Cambridge, MA, USA, 2001.
23. Landau, L.D.; Lifshitz, E.M. *Quantum Mechanics*; Pergamon: Oxford, UK, 1977.
24. Wang, W.; Yang, H.; Tang, P.; Zhao, C.; Gao, J. Soliton trapping of dispersive waves in photonic crystal fiber with two zero dispersive wavelengths. *Opt. Express* **2013**, *21*, 11215–11226. [CrossRef] [PubMed]